PAPER

A novel cage for actinides: $A_6W_4Al_{43}$ (A = U and Pu)

View the article online for updates and enhancements.

IOP ebooks™

Bringing you innovative digital publishing with leading voices to create your essential collection of books in STEM research.

Start exploring the collection - download the first chapter of every title for free.

A novel cage for actinides: $A_6W_4Al_{43}$ (A = U and Pu)

K Huang[1]**, W L Nelson**[1,2]**, A T Chemey**[3]**, T E Albrecht-Schmitt**[3]
and R E Baumbach[1,2,4]

[1] National High Magnetic Field Laboratory, Florida State University, Tallahassee, FL 32306,
United States of America
[2] Department of Physics, Florida State University, Tallahassee, FL 32306, United States of America
[3] Department of Chemistry, Florida State University, Tallahassee, FL 32306, United States of America

E-mail: baumbach@magnet.fsu.edu

CrossMark

Abstract

We report on synthesis and characterization of the compounds $A_6W_4Al_{43}$ (A = U and Pu), that form in the hexagonal $Ho_6Mo_4Al_{43}$ caged-structure family. The A ions reside within W/Al cages where the A–A nearest neighbors form dimers between adjacent W/Al cages, with U–U and Pu–Pu distances of 3.3892 Å and 3.4080 Å, respectively. While the W/Al networks provide environments similar to those of other cage-like materials (e.g. filled skutterudites), the atomic displacement parameters from single crystal x-ray diffraction measurements show that the A-ions do not exhibit rattling behavior. We find that there is site interchange disorder on one of the W/Al sites. Magnetic susceptibility measurements show that $U_6W_4Al_{43}$ displays anisotropic Curie–Weiss behavior where it fits to the data yield an effective magnetic moment near 2.0 μ_B/U. At low temperatures the magnetic susceptibility deviates from the Curie–Weiss temperature dependence and eventually saturates to a constant value. In contrast, $Pu_6W_4Al_{43}$ displays nearly temperature independent Pauli paramagnetism for all temperatures, as would be expected if the $5f$-electrons are delocalized. The electrical resistivity for $U_6W_4Al_{43}$ increases slightly with the decreasing temperature, suggesting that it is dominated by f-electronic hybridization effects and disorder scattering that originates from the W/Al site interchange. Specific heat measurements for $U_6W_4Al_{43}$ further reveal an enhanced electronic Sommerfeld coefficient that is consistent with a moderately enhanced charge carrier effective mass. Together these measurements expose these materials as hosts for unstable f-electron magnetism, where the novel cage-like structures control the phenomena through the spacing between the A ions. Through this combination of mild magnetism, the low cost elements of the Al–W cages, and chemical tunability that has been shown for related materials in the same structure, the $A_6W_4Al_{43}$ compounds emerge as promising nuclear waste-forms for transuranics, while the wider family of materials makes an appealing environment for studying f-electron physics in a novel structure.

Keywords: strongly correlated electrons, actinide, magnetism, cage-like compounds

(Some figures may appear in colour only in the online journal)

1. Introduction

The task of developing and improving sustainable energy sources is of paramount importance. One of the oldest examples is nuclear energy, having been harnessed for almost a century. However a persistent problem is how to manage the long-lived radioactive and toxic by-products that results from its use. As a result, it is crucial to find new materials that can host actinides with improved long-term stability against radiation damage or other environmental conditions: e.g. exposure to water. Caged-like intermetallic structures are promising candidates due to their environmental stability and chemical

diversity, which together provide a high degree of control of electronic and thermodynamic properties.

There are many different families of cage-like materials, including those with the formula AT_2M_{20} (A = alkali earth/metals, rare earths, actinides, T = transition metals, M = Al, Zn, Cd) [1–3], clathrates [4, 5], and filled skutterudites [6]. Cage-like structures often feature novel behavior when a large mass ion is present inside the cages. If the heavy ion is loosely bound to the cage, this may lead to 'rattling' behavior that strongly scatters phonons and produces enhanced thermoelectric properties [7, 8]. In addition to this, the $5f$ electrons from the actinide elements are a deep reservoir for novel physics, where a variety of emergent macroscopic states are generated from the variable hybridization of f-electron with other d- and s/p-electrons [9]. Examples include UCoGe and URhGe which are exotic ferromagnetic superconductors [10, 11], PuCoGa$_5$ which superconducts at T_c = 18.5 K (roughly five times higher than the other MTX_5 superconductors) [12, 13], and URu$_2$Si$_2$ which hosts the enigmatic hidden order state and unconventional superconductivity [14–16]. These behaviors are reminiscent of what is seen in other strongly correlated f-electron materials, including CeCu$_2$Si$_2$ [17–19], and for all such systems it remains an ongoing challenge to understand the details of how interactions between the f- and other electrons produces the multitude of behaviors that are observed.

In this manuscript we report the synthesis and behavior of two compounds $A_6W_4Al_{43}$ (A = U and Pu) that form from an aluminum molten metal flux in the cage-containing Ho$_6$Mo$_4$Al$_{43}$-type structure (space group $P6_3/mcm$) [2, 3, 20–22]. While the cage-like W/Al environment might be expected to encourage rattling behavior of the U/Pu ions, inspection of the atomic displacement parameters indicates rigid bonds amongst all atoms in the lattice. The nearest neighbor U–U and Pu–Pu pairs have a spacing of 3.3892 Å and 3.4080 Å and each set of pairs (dimers) are separated by 5.508 Å and 5.5120 Å, respectively. According to the Hill plot (for uranium), this places these materials close to the A–A distance where the f-electrons are expected to be either weakly magnetic or delocalized [9, 23]. DC magnetic susceptibility measurements support this scenario, revealing anisotropic Curie–Weiss paramagnetism that saturates at low temperatures for U$_6$W$_4$Al$_{43}$ and enhanced Pauli paramagnetism for Pu$_6$W$_4$Al$_{43}$. In addition, for U$_6$W$_4$Al$_{43}$ electrical resistivity measurements suggest hybridization between f- and conduction electron states with strong disorder scattering, while heat capacity measurements uncover Fermi liquid behavior with an enhanced electronic coefficient $\gamma = 70$ mJ mol^{-1} K^2 per U. Taken together, these qualities indicate that this structure may be suitable as a nuclear waste form because the magnetism is simple and mild, the material is predominantly constructed from aluminum, and the A-site likely will host many different mixtures of actinide elements. Furthermore, the wider family of materials is an appealing environment for studying f-electron physics in a novel structure.

2. Experimental details

As ^{239}Pu($t_{1/2}$ = 24 065 years) is potentially hazardous owing to its toxicity as well as α emission all handling of plutonium and the plutonium-containing compounds were conducted in a laboratory at Florida State University specialized to perform investigations on transuranium elements. Special precautions were also taken for magnetic measurements, which were performed in a Quantum Design MPMS3. For all of the magnetic measurements on ^{239}Pu the samples were placed in a sealed polytetrafluoroethylene (PTFE) sample holder. One such holder is displayed in figure 3(c), where the samples are in the orange colored section at the top of the panel.

$A_6W_4Al_{43}$ (A = U and Pu) single crystals were synthesized using an aluminum molten metal flux [24, 25]. The starting materials were uranium/plutonium metal from Los Alamos National Laboratory, tungsten wire purchased from Cleveland Wire Plant, and aluminum shot (5N) from Alfa Aesar. Starting materials were weighed in the molar ratio of 2:1:50 (A:W:Al), placed in an alumina crucible purchased from CoorsTek, and then sealed in vacuum in a quartz tube. The mixture was heated up to 1000 °C, dwelled at 1000 °C for 72 h, and slow cooled at a rate of 3 °C h^{-1} down to 850 °C where they were removed from the furnace. The Al flux was removed by immersing the reacted material in dilute HCl which revealed acid resistant $A_6W_4Al_{43}$ crystals (figures 1(a) and (b)). It should be noted that the Th and Np members were attempted using the same synthesis method but resulted in ThW$_2$Al$_{10}$ (which is itself a new material[5]) and an unidentified Np compound (starting material NpO$_2$).

The synthesis of Pu$_6$W$_4$Al$_{43}$ required adherence to several additional details. Firstly due to the scarcity of Pu metal the batch size was reduced from that of the U analogue: i.e. whereas a typical U-containing batch used 0.5–1.0 g of depleted uranium, the Pu-containing batches used 100 mg of metallic plutonium. As a result, U- and Pu-containing batches were reacted in 2 ml and 0.5 ml alumina crucibles, respectively. Another important aspect of the synthesis is that the Pu was placed in the middle of the crucible between two layers (top/bottom) of the aluminum flux. A first synthesis attempt was performed where the Pu was placed on the top of the crucible while the Al and W were placed in the middle and bottom of the crucible. This approach produced large amounts of single crystalline WAl$_4$. Because of the crucible's confined shape (as can be seen in figure 1(c)) the WAl$_4$ formed before the Pu could be integrated into the melt. In the subsequent attempt the W and Pu were placed in close proximity at the center of the crucible with aluminum both above and below them. This resulted in significant yields of single crystalline Pu$_6$W$_4$Al$_{43}$ that form in hexagonal rods as can be seen in figure 1(b) (trace amounts of single crystalline WAl$_4$ was still observed).

X-ray diffraction measurements were performed at room temperature using a Bruker D8 Quest with an area detector. Magnetization measurements were performed in a Quantum Design MPMS3 VSM, using a conventional quartz sample holder for an oriented single crystal of U$_6$W$_4$Al$_{43}$. Measurements for Pu$_6$W$_4$Al$_{43}$ were performed on a collection of unaligned single crystals, four days after the synthesis was completed to limit the effects of radiation damage. A

---

[5] The crystallographic information file (CIF) for ThW$_2$Al$_{10}$ is available from the Cambridge Crystal Structure Database Center with collection number 1870903.
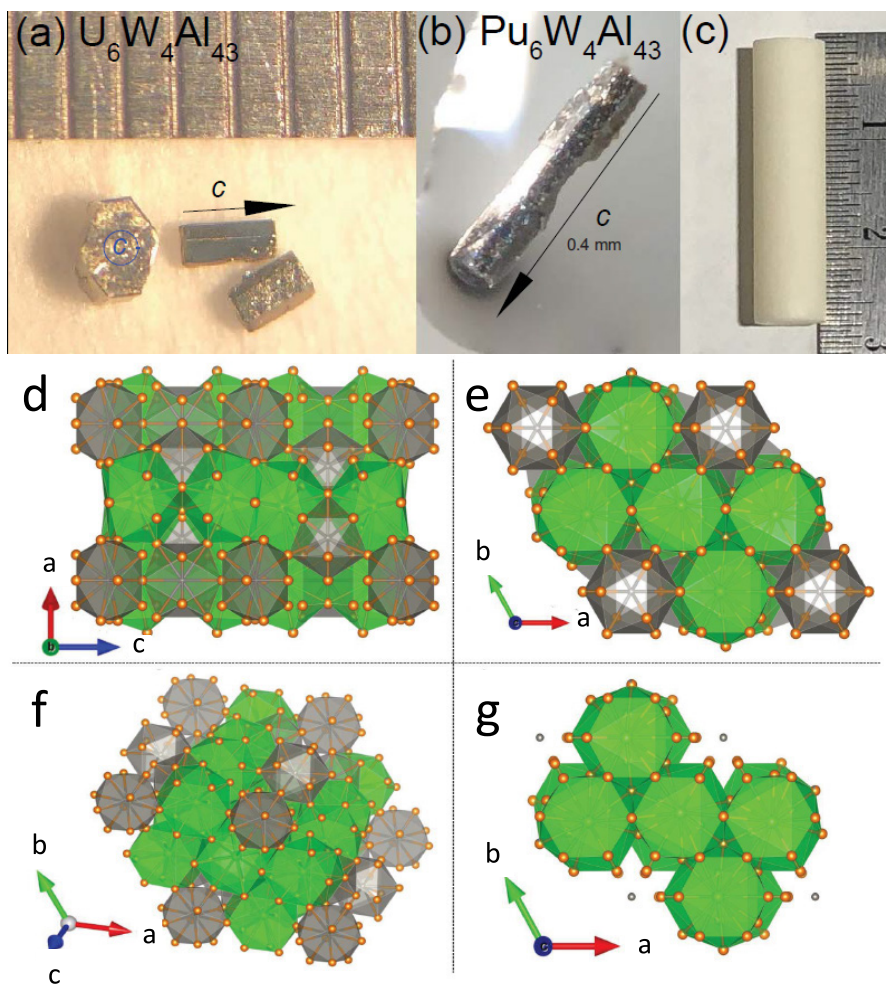
Figure 1. Representative hexagonal crystals of $U_6W_4Al_{43}$ and $Pu_6W_4Al_{43}$ in panels (a) and (b), respectively. The markings in (a) are in units of half a mm. The $Pu_6W_4Al_{43}$ single crystals are approximately 0.4 mm. (c) 0.5 ml alumina crucible used for synthesis of $Pu_6W_4Al_{43}$ with the ruler in units of cm. Note how the length of the crucible is significantly larger than the radius. One end of the crucible is closed. (d) *c*-axis in (e), 1 1 1-direction in (f), and *c*-axis without the tungsten polyhedra for clarity in (g). The U/Pu site is represented by the green dots, tungsten by gray, and aluminum sites by orange.

background signal from the Quantum Design PTFE sealed sample holder was removed by performing two scans and subtracting the difference, where the first scan had 5.5 mg of $Pu_6W_4Al_{43}$ and the second measurement was performed when the holder contained 25.2 mg. The two scans were performed one day apart with the background subtracted data represented by the purple data in figure 3(a). DC electrical resistivity measurements for $U_6W_4Al_{43}$ were performed for $U_6W_4Al_{43}$ in a Quantum Design PPMS down to 1.8 K using the standard four-wire method. Specific measurements were also performed for $U_6W_4Al_{43}$ in a Quantum Design PPMS using a conventional thermal relaxation technique.

3. Results

Refinement of the single crystal x-ray diffraction data reveals close agreement with the hexagonal $Ho_6Mo_4Al_{43}$ prototype structure (space group $P6_3/mcm$) [2], with lattice parameters $a = 10.9617(2)$ Å and $c = 17.6984(3)$ Å for the U-compound and $a = 10.9776(8)$ Å and $c = 17.718(1)$ Å for the

Pu-compound. The crystallographic results are displayed in Table 1 for both compounds. Tables 2 and 3 display the atomic positions for U6W4Al43 and Pu6W4Al43, respectively. As shown in figures 1(d)–(g), the U/Pu atoms are coordinated by 24 lighter atoms, where the U/Pu–Al bond distances range from 3.048(2) Å to 3.229(3) Å. The occupancy fits display very small deviations for all sites except for Al, which shows a small interchange with W on the order of 11.8% and 8.1% on the W3/Al7 sites for $U_6W_4Al_{43}$ and $Pu_6W_4Al_{43}$, respectively. Attempts to fit the data using full Al occupancy result in a non-physical negative atomic displacement parameter U_{iso} for Al7. Given the dissimilar reactivity and structural chemistry of aluminum and tungsten, the small substitution level is reasonable. We note that off-stoiciometric variants were already observed in other members of this structure, including $Er_6Cr_{5.96}Al_{41.04}$ and $Lu_6Cr_{6.76}Al_{40.24}$ [26]. Also noteworthy is that unlike other caged compounds, the U/Pu atom position is well-defined with a very low thermal displacement of $U_{iso} = 0.001$ Å^2, showing no evidence of atomic-site 'rattling'. By comparison, the thermal displacement parameters for 'rattling' atoms in other cage-like structures are larger: e.g. $U_{iso} = 0.05$ Å^2 for Tl
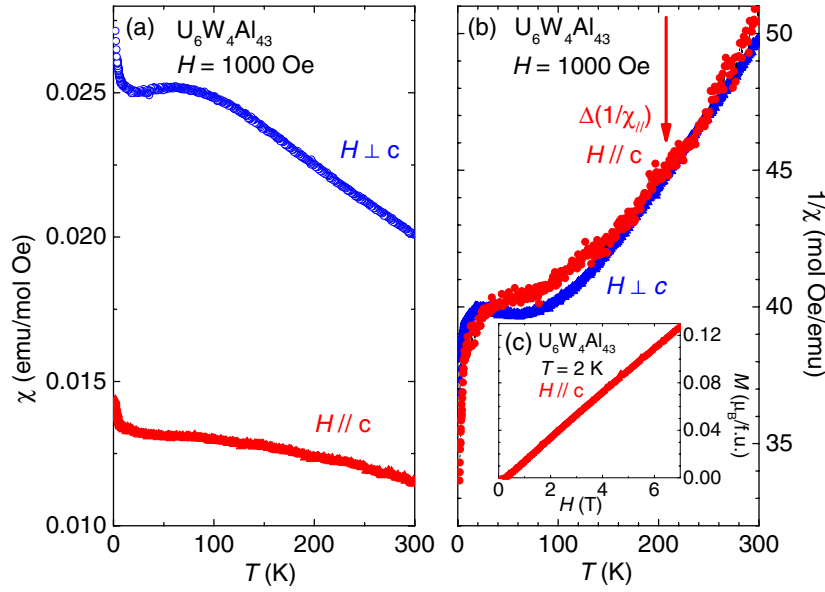
Figure 2. (a) DC magnetic susceptibility χ data under a magnetic field $H = 1000$ Oe and down to temperature $T = 2$ K for $U_6W_4Al_{43}$ with $H \mathbin{/\!/} c$ and $H \perp c$. Both orientations show Curie–Weiss behavior at high temperatures (250 K and above) and approach a temperature-independent region at lower temperatures. For $H \perp c$ there is a broad peak centered near $T = 50$ K. (b) Curie–Weiss fits were performed on the inverse magnetic susceptibility $(1/\chi)$ for $T \geqslant 250$ K. For clarity, the dataset with $H \perp c$ was shifted by a constant. Both orientations display a similar Curie–Weiss temperature dependence, with $\mu_{\mathrm{eff}} = 2$ and 1.8 μ_B/U for $H \perp c$ and $H\mathbin{/\!/}c$, respectively. (c) Magnetization M as a function of H for $U_6W_4Al_{43}$ with $H \perp c$ at $T = 2$ K, showing clear paramagnetic behavior up to 7 T.

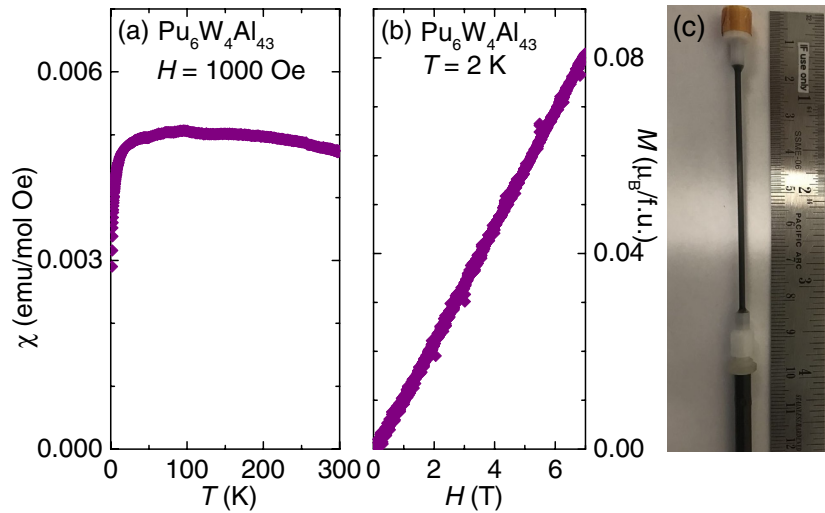**Figure 3.** (a) DC magnetic susceptibility χ data under a magnetic field $H = 1000$ Oe and down to temperature $T = 2$ K for $Pu_6W_4Al_{43}$. For the entire temperature range measured, a clear temperature-independent Pauli paramagnetism is observed with $\chi_0 \sim 0.5 \cdot 10^{-2}$ emu/mol Oe. This value is significantly larger than more conventional Pauli paramagnets such as Li [36]. (b) Magnetization $Pu_6W_4Al_{43}$ at $T = 1.8$ K with H sweeping from 0 T up to 7 T, showing a linear behavior that is expected for Pauli paramagnetism. (c) Example of the type of PTFE sealed sample holder used for the magnetization measurements on $Pu_6W_4Al_{43}$. This is important as Pu-containing samples present radiation and toxic hazards.

in the skutterudite $Tl_{0.22}Co_4Sb_{12}$ or $U_{\mathrm{iso}} = 0.15$ Å^2 for Eu in the clathrate $Eu_8Ga_{16}Ge_{30}$ [8, 27].

The magnetic susceptibilities χ versus temperature T data for both $U_6W_4Al_{43}$ and $Pu_6W_4Al_{43}$ are shown in figures 2 and 3, respectively. For $U_6W_4Al_{43}$ the measurements were performed with magnetic fields applied parallel ($/\!/$) and perpendicular ($\perp$) to the crystalline c-axis, where the directions are easily identified because the crystals form as rods with clear hexagonal cross sections (see figure 1(a)). Displayed in figure 2(b)

is the inverse magnetic susceptibility $(1/\chi)$ for both orientations. The dataset with $H \perp c$ was offset by a value $\Delta\chi = 36$ (mol Oe/emu) to more clearly illustrate the similar slopes of both datasets. Analysis of Curie–Weiss fits performed above 250 K yield effective magnetic moments in terms of the Bohr magneton, μ_B, as $\mu_{\mathrm{eff}} = 2.0$ and 1.8 μ_B/U for $H \perp c$ and $H\mathbin{/\!/}c$, respectively which are suppressed from the values expected for tetravalent uranium ($\mu_{\mathrm{eff}} \approx 3.6\mu_B$). We also find large and negative Curie–Weiss temperatures $\theta = -600$ and -940 K for $H \perp c$ and $H\mathbin{/\!/}c$, respectively. Similar values have previously
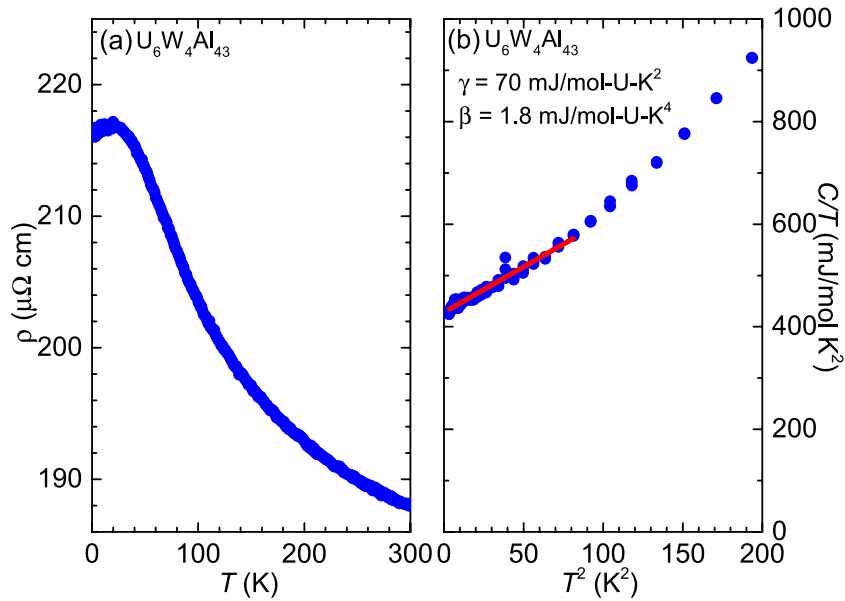
Figure 4. (a) Temperature T dependence of the electrical resistivity ρ for an unaligned crystal of $U_6W_4Al_{43}$. $\rho(T)$ displays a broad maximum centered at $T = 50$ K that is consistent with Kondo lattice behavior and significant electron scattering due to disorder. (b) Specific heat measurements plotted as C/T versus T^2 for a single crystal of $U_6W_4Al_{43}$ down to $T = 1.8$ K. The solid line is a fit to the data, as described in the text.

been observed in other U- and Ce-based materials and are an indication of strong electronic correlations, rather than the strength of the magnetic exchange interaction [28]. In addition to this, crystal electric field (CEF) splitting of the f-states would cause a strong deviation from Curie–Weiss behavior for temperatures that are not well above the CEF energy scale. This likely necessitate measurements to much higher temperatures. At temperatures below 50 K, $\chi(T)$ saturates towards temperature independent values (2.5 and $1.3 \cdot 10^{-2}$ (emu/mol Oe) for $H \perp c$ and $H//c$, respectively). This type of behavior has been seen previously in U-based materials with strong electronic correlations, weak magnetism, and an unstable f-electron valence: e.g. $U(Fe,Re)_2Al_{10}$ [29, 30], and U_2RuGa_8 [31]. Finally, at the lowest temperatures, there is a weak upturn that is likely due to the presence of a small concentration of paramagnetic impurities. Magnetization measurements at constant temperature were performed at $T = 1.8$ K and are displayed in figure 2(c), showing a linear dependence with increasing field that is indicative of paramagnetism.

Unlike its U-relative, $\chi(T)$ for $Pu_6W_4Al_{43}$ is nearly temperature independent across all temperatures with a value $0.5 \cdot 10^{-2}$ emu/mol Oe (figure 3(a)). This reveals Pauli-paramagnetism, similar to what is seen for $Pu_{0.8}V_2Al_{20}$ [32], and the Pu monochalcogenides ($PuCh$, $Ch = $ S, Se, and Te) where the f-orbitals are delocalized [33–35]. Note that, like other 5f-based Pauli paramagnets, the amplitude of χ is larger than that of more conventional Pauli paramagnets such as Li with $\chi_p = 2.08 \cdot 10^{-6}$ emu/mol Oe [36]. This occurs because the delocalized f-electrons contribute an enhanced density of states at the Fermi energy, and thereby enhance the magnetic susceptibility via the expression $\chi_P = \mu_0\mu_B^2 N(E_F)$, where μ_0 is vacuum permeability and $N(E_F)$ is the electronic density of states at the Fermi energy. Note that at the lowest temperatures

Table 1. Crystallographic information and data for $U_6W_4Al_{43}$ and $Pu_6W_4Al_{43}$.

Formula	$U_6W_4Al_{43}$	$Pu_6W_4Al_{43}$
Crystal system	Hexagonal	Hexagonal
Structure type	$Ho_6Mo_4Al_{43}$	$Ho_6Mo_4Al_{43}$
Space group	$P6_3/mcm$	$P6_3/mcm$
Formula units/cell (Z)	$Z = 2$	$Z = 2$
a (Å)	10.9617(2)	10.9776(8)
c (Å)	17.6984(3)	17.7182(13)
V (Å^3)	1841.71(7)	1849.1(3)
pcalcd (g cm^{-3})	5.994	6.012
μ (mm^{-1})	39.751	23.952
$F(000)$	2814	2838
Unique Reflns	1496	836
GOF on F^2	1.093	1.363
R_{int}	0.0852	0.0420
R_1 ($I > 2\sigma(l)$)	0.0179	0.0265
wR_2 (all data)	0.0366	0.0629

$\chi(T)$ decreases strongly. The origin of this behavior is not clear, but it may originate from difficulty in subtracting the background magnetism of the teflon sample holder. Magnetization versus field measurements at $T = 1.8$ K are displayed in figure 3(b). There is a linear dependence of the magnetization with increasing H, consistent with the behavior for a Pauli paramagnet due to Zeeman splitting of the conduction bands.

For $U_6W_4Al_{43}$, the electrical resistivity weakly increases with decreasing temperature and eventually saturates to a value near 180 $\mu\Omega$ cm at low temperature (figure 4(a)). This increase in $\rho(T)$ is similar to what is seen in similar materials

Table 2. Atomic parameters of $U_6W_4Al_{43}$.

Atom	Wyckoff site	x	y	z	Occupancy	U_{eq}
U	12k	0.471 26(2)	0	0.905 92(2)	1	0.006 21(4)
W(1)	6g	0.267 98(2)	0	0.75	1	0.000 354(5)
W(2)	2b	0	0	0.5	1	0.003 48(7)
Al(1)	12j	0.551 17(16)	0.145 51(17)	0.75	1	0.0077(3)
Al(2)	12k	0.162 42(14)	0	0.613 10(8)	1	0.0081(3)
Al(3)	24l	0.764 85(11)	0.247 52(8)	0.837 32(6)	1	0.007 77(18)
Al(4)	6g	0	−0.1498(2)	0.75	1	0.0078(4)
Al(5)	12k	0.256 69(14)	0	0.470 89(2)	1	0.0076(2)
Al(6)	12i	0.495 03(16)	0.247 52(8)	0.5	1	0.0093(3)
Al(7)	8h	0.6667	0.3333	0.869 73(6)	0.8822(17)	0.0071(3)
W(3)	8h	0.6667	0.3333	0.869 73(6)	0.1178(17)	0.0071(3)

Table 3. Atomic parameters of $Pu_6W_4Al_{43}$.

Atom	Wyckoff site	x	y	z	Occupancy	U_{eq}
Pu	12k	0.470 70(3)	0	0.405 56(2)	1	0.004 96(13)
W(1)	6g	0.267 62(5)	0	0.25	1	0.000 254(15)
W(2)	2b	0	0	0.5	1	0.0028(2)
Al(1)	12j	0.4049(3)	−0.1455(4)	0.25	1	0.0065(6)
Al(2)	12k	0.1612(3)	0	0.386 38(18)	1	0.0069(6)
Al(3)	24l	0.3951(2)	0.2357(3)	0.336 87(14)	1	0.0077(5)
Al(4)	6g	0	−0.1494(5)	0.25	1	0.0075(9)
Al(5)	12k	0.2553(3)	0	0.5297(2)	1	0.0069(6)
Al(6)	12i	0.4949(3)	0.247 44(17)	0.5	1	0.0088(6)
Al(7)	8h	0.6667	0.3333	0.370 79(15)	0.919(4)	0.0065(9)
W(3)	8h	0.6667	0.3333	0.370 79(15)	0.081(4)	0.0065(9)

(e.g. $U(Fe,Ru)_2Al_{10}$ [29, 30, 37] and U_2RuGa_8 [31]) and may indicate that there are Kondo-like interactions that influence the electrical transport. From here, it is possible that the saturation to an enhanced low temperature residual resistivity should be understood to result from disorder scattering due to the W/Al site interchange. While this seems like the most likely scenario, we point out that U_2Ru_2Sn exhibits a similar evolution [38]. Here, it has proposed that the saturating low temperature electrical resistivity is not due to impurity scattering, but rather represents an intrinsic Kondo insulating behavior [38, 39]. This is an intriguing possibility since it has been proposed by Dzero *et al* [40] that Kondo insulators might be environments for topologically protected electronic states: e.g. as for SmB_6 [41]. Further work is needed to explore this scenario in $U_6W_4Al_{43}$.

Finally, the temperature dependence of the heat capacity for $U_6W_4Al_{43}$ is shown in figure 4(b), where Fermi liquid behavior that is described by the expression $C/T = \gamma + \beta T^2$ is observed. Fits to the data yield an electronic heat capacity coefficient of $\gamma = 70$ mJ mol^{-1} K^2 per U, suggesting a moderately enhanced electron mass. A Debye temperature $\Theta_D \approx 388$ K is calculated using the relation $\theta_D = (1944 \cdot n/\beta)^{1/3}$ where $n = 53$, the number of atoms per formula unit. This is a reasonable value for Θ_D and is similar to other actinide-based cage-like structures such as (Th, U)Ir_2Zn_{20} ($\Theta_D = 296$ K and 283 K, respectively) or filled skutterudites such as $ThPt_4Ge_{12}$ ($\Theta_D = 217$ K) [42, 43].

4. Discussion

The compounds $U_6W_4Al_{43}$ and $Pu_6W_4Al_{43}$ both exhibit properties that are consistent with the broader class of actinide systems whose phenomenology is described by the Hill plot [9, 23]. The Hill plot is a phenomenological picture, where the degree of overlap between the *f*-electron wave functions of neighboring atoms establishes whether a compound is magnetic or nonmagnetic: e.g. for U-based materials if the *A–A* nearest neighbor distance d_{A-A} is less than 3.5 Å then the *f*-electrons have a tendency to delocalize [9]. For $U_6W_4Al_{43}$ and $Pu_6W_4Al_{43}$ $d_{A-A} = 3.3892$ Å and 3.4080(6) Å, respectively, placing them at the border between localized *f*-moment magnetism and delocalized *f*-moment Pauli paramagnetism. For $U_6W_4Al_{43}$, the result is that Curie–Weiss behavior occurs at higher temperature where the effective magnetic moment is reduced from the value expected for tetravalent uranium and the Curie–Weiss temperature is large and negative. Similar behavior has been observed previously in similar materials such as $U(Fe,Ru)_2Al_{10}$ and U_2RuGa_8 where the instability of the *f*-electron valence dominates the behavior [29–31]. It is also likely that crystal electric field splitting of the Hund's rule multiplet plays a role in this temperature dependence. In contrast, Pauli-paramagnetism is observed in $Pu_6W_4Al_{43}$ for all temperatures, suggesting that the 5*f* electrons are delocalized. These behaviors are of interest because both nearly localized *f*-electron and delocalized/itinerant electronic

behavior sometimes results in unusual phenomena: e.g. many *f*-electron superconductors are found on the border of a magnetic or valence instability such as $CeCoIn_5$ and $PuCoGa_5$ [44, 45]. An important example is $PuCoGa_5$ which hosts unconventional superconductivity at an anomalously high temperature, whose origin is still under debate [12, 13]. Although no superconductivity has yet been observed for $U_6W_4Al_{43}$, $Pu_6W_4Al_{43}$, or other compounds in this structure, further investigations in this family would be attractive. We also point out that the electrical transport behavior may indicate Kondo insulating behavior, but further work is needed to test this scenario.

Since the behavior of these systems is understood in the context of the Hill plot, where both systems are in the crossover region between nonmagnetic and magnetic behavior, it is interesting to consider tuning the *A*–*A* spacing to control the *f*-state. For instance, if the *A*–*A* spacing could be increased then the *f*-moments would tend to localize. In this scenario there might first emerge a quantum phase transition that might be surrounded by a region of novel behavior [46]. Further expansion of the *A*–*A* spacing would subsequently result in complex magnetism involving both *A*–*A* inter-dimer interactions. There are multiple potential tuning avenues including chemical substitution on the W and Al sites. Earlier studies of the $A_6T_4Al_{43}$ family reveal the feasibility of this approach since it has already been shown that this structure readily forms with other transition metals such as Cr, Ti, V, Nb, Ta, and Mo [2, 22]. Furthermore, Al is one of the smaller elements that comprises the majority of the structure and it might be possible to partially substituted with either Ga or In and thereby isovalently expand the lattice.

5. Conclusion

We have presented results for two actinide-compounds that form in the hexagonal $Ho_6W_4Al_{43}$ type cage-structure. Thermodynamic and magnetic measurements reveal behavior that is consistent with weak *f*-electron magnetism and hybridization effects that result from the compounds' positions in the Hill plot. Furthermore, these compounds feature some characteristics that make them desirable as potential nuclear waste forms: (1) they are predominantly comprised of abundant elements (Al and W). (2) The synthesis technique is widely accessible, utilizing temperatures that are easily achieved by conventional commercially available furnaces using the flux method, which is forgiving to the inclusion of oxygen impurities. (3) The compound shows stability when exposed to air, water, and hydrochloric acid. (4) Importantly, the material, and therefore its properties, are highly tunable as member-compounds using different transition metals. This has already been reported.

Acknowledgments

ORCID iDs

R E Baumbach ● https://orcid.org/0000-0002-6314-3629

References

[1] Nasch T, Jeitschko W and Rodewald U C 1997 *Z. Naturforsch.* **52b** 1023
[2] Niemann S and Jeitschko W 1995 *J. Solid State Chem.* **116** 131
[3] Thiede V M T, Jeischko W, Niemann S and Ebel T 1998 *J. Alloys Compd.* **267** 23
[4] Sales B C, Chakoumakos B C, Keppens V, Jin R, Mandrus D and Thompson J R 2001 *Mat. Res. Soc. Symp. Proc.* 691 G7.2.1
[5] Beekman M, Wei K and Nolas G S 2016 *Appl. Phys. Rev.* **3** 040804
[6] Sato H, Suguwara H, Aoki Y and Harima H 2009 *Handbook of Magnetic Materials* vol 18 (Amsterdam: Elsevier)
[7] Sales B C, Mandrus D and Williams R K 1996 *Science* **272** 1325
[8] Sales B C, Chakoumakos B C and Mandrus D 2000 *Phys. Rev.* B **61** 2475
[9] Moore K T and van der Laan G 2009 *Rev. Mod. Phys.* **81** 235
[10] Aoki D, Huxley A, Ressouche E, Braithwaite D, Flouquet J, Brison J-P, Lhotel E and Paulsen C 2001 *Nature* **413** 613
[11] Huy H T, Gasparini A, de Nijs D E, Huang Y, Klaasse J C P, Gortenmulder T, Visser A, Hamann A, Görlach T and Löhneysen H V 2007 *Phys. Rev. Lett.* **99** 067006
[12] Sarrao J L, Morales L A, Thompson J D, Scott B L, Stewart G R, Wastin F, Rebizant J, Boulet P, Colineau E and Lander G H 2002 *Nature* **420** 297
[13] Curro N J, Caldwell T, Bauer E D, Morales L A, Graf M J, Bang Y, Balatsky A V, Thompson J D and Sarrao J L 2005 *Nature* **434** 622
[14] Maple M B, Chen J W, Dalichaouch Y, Kohara T, Rossel C, Torikachvili M S, McElfresh M W and Thompson J D 1986 *Phys. Rev. Lett.* **56** 185
[15] Palstra T T M, Menovsky A A, van den Berg J, Dirkmaat A J, Kes P H, Nieuwenhuys G J and Mydosh J A 1985 *Phys. Rev. Lett.* **55** 2727
[16] Mydosh J A and Oppeneer P M 2014 *Phil. Mag.* **94** 3642
[17] Steglich F, Aarts J, Bredl C D, Lieke W, Meschede D, Franz W and Schäfer H 1979 *Phys. Rev. Lett.* **43** 1892
[18] Yuan H Q, Grosche F M, Deppe M, Geibel C, Sparn G and Steglich F 2003 *Science* **302** 2104
[19] Steglich F 2012 *J. Phys.: Condens. Matter* **400** 022111
[20] Wolff M W, Niemann S, Ebel T and Jeitschko W 2001 *J. Magn. Magn. Mater.* **223** 1
[21] Condron C L, Strand J D, Canfield P C and Miller G J 2003 *Acta Cryst.* E **59** i147
[22] Fushiya K, Miyazaki R, Higashinaka R, Matsuda T D and Aoki Y 2014 *JPS Conf. Proc.* 3 011018
[23] Hill H H 1970 *Plutonium 1970 and Other Actinides* vol 17, ed W H Miner (New York: AIME) p 2
[24] Canfield P C and Fisk Z 1995 *Phil. Mag.* B **65** 1117
[25] Kanatzidis M G, Pöttgen R and Jeitschko W 2005 *Angew. Chem. Int. Ed.* **44** 6996
[26] Yanson T I, Manyako M B, Bodak O I, Cerny R, Pacheco J V and Yvon K 1994 *Z. Kristallogr.* **209** 922

[27] Sales B C, Chakoumakos B C, Jin R, Thompson J R and Mandrus D 2001 *Phys. Rev.* B **63** 245113

[28] Sereni J G, Westerkamp T, Küchler R, Caroca-Canales N, Gegenwart P and Geibel C 2007 *Phys. Rev.* B **75** 024432

[29] Troć R, Samsel-Czekala M, Talik E, Wawryk R, Gajek Z and Pasturel M 2015 *Phys. Rev.* B **92** 104427

[30] Troć R, Pasturel M, Samsel-Czekala M, Wawryk R and Gajek Z 2018 *J. Alloys Compd.* **01** 319

[31] Troć R, Bukowski Z, Sułkowski C, Morkowski A, Szajek J A and Chełkowska G 2005 *Physica* B **359** 1375–7

[32] Winiarski M J, Griveau J-C, Colineau E, Wochowski K, Wisniewski P, Kaczorowski D, Caciuffo R and Klimczuk T 2017 *J. Alloys Compd.* **696** 1113

[33] Lander G H, Rebizant J, Spirlet J C, Delapalme A, Brown P J, Vogt O and Mattenberger K 1987 *Physica B + C* **146** 341

[34] Fournier J M, Pleska E, Chiapusio J, Rossat-Mignod J, Rebizant J, Spirlet J C and Vogt O 1990 *Physica* B **163** 493

[35] Santini P, Lémanski R and Erdős P 1998 *J. Alloys Compd.* **267** 23

[36] Schumacher R T and Slichter C P 1956 *Phys. Rev.* **101** 58

[37] Troć R, Pasturel M, Tougait O, Potel M and Noël H 2011 *Intermetallics* **19** 913

[38] Paschen S, Tran V H, Senthilkumaran N, Baenitz M, Steglich F, Strydom A M, du Plessis P D V, Motoyama G and Sato N K 2003 *Physica* B **329** 549

[39] Niklowitz P G, Beckers F, Lonzarich G G, Knebel G, Salce B, Thomasson J, Bernhoeft N, Braithwaite D and Flouquet J 2005 *Phys. Rev.* B **72** 024424

[40] Dzero M, Xia J, Galitski V and Coleman P 2016 *Annu. Rev. Condens. Matter Phys.* **7** 249

[41] Takimoto T 2011 *J. Phys. Soc. Japan* **80** 123710

[42] Swatek P, Daszkiewicz M and Kaczorowski D 2012 *Phys. Rev.* B **85** 094426

[43] Kaczorowski D and Tran V H 2008 *Phys. Rev.* B **77** 180504

[44] Löhneysen H, Rosch A, Vojta M and Wölfle P 2007 *Rev. Mod. Phys.* **79** 1015

[45] Pfleiderer C 2009 *Rev. Mod. Phys.* **81** 1551

[46] Maple M B, Baumbach R E, Butch N P, Hamlin J J and Janoschek M 2010 *J. Low Temp. Phys.* **161** 4